processes

MDPI

Article

Controlled Synthesis of Triangular Silver Nanoplates by Gelatin–Chitosan Mixture and the Influence of Their Shape on Antibacterial Activity

Quoc Khuong Vo [1], Duc Duy Phung [2], Quynh Nhu Vo Nguyen [3], Hong Hoang Thi [4], Nhat Hang Nguyen Thi [5], Phuong Phong Nguyen Thi [1,*], Long Giang Bach [6,7] and Lam Van Tan [8,9]

1 Faculty of Chemistry, Ho Chi Minh City University of Science, Vietnam National University, Ho Chi Minh City 70000, Vietnam; vqkhuong@hcmus.edu.vn
2 Faculty of Biology and Biotechnology, Ho Chi Minh City University of Science, Vietnam National University, Ho Chi Minh City 70000, Vietnam; ducduy001@gmail.com
3 Faculty of Materials Engineering, University of Technology of Hochiminh City, Ho Chi Minh City 70000, Vietnam; vqnhu.1512@gmail.com
4 Faculty of Pharmacy, Nguyen Tat Thanh University, Ho Chi Minh City 70000, Vietnam; hthong@ntt.edu.vn
5 Falcuty of Natural Sciences, Thu Dau Mot University, Binh Duong Province 75000, Vietnam; hangntn@tdmu.edu.vn
6 Center of Excellence for Functional Polymers and NanoEngineering, Nguyen Tat Thanh University, Ho Chi Minh City 70000, Vietnam; blgiang@ntt.edu.vn
7 Center of Excellence for Green Energy and Environmental Nanomaterials, Nguyen Tat Thanh University, Ho Chi Minh City 70000, Vietnam
8 NTT Hi-Tech Institute, Nguyen Tat Thanh University, Ho Chi Minh City 70000, Vietnam; lamvantan101076@gmail.com
9 Ben Tre's Department of Science and Technology, Ben Tre Province 930000, Vietnam
* Correspondence: ntpphong@hcmus.edu.vn

Received: 21 October 2019; Accepted: 11 November 2019; Published: 21 November 2019

Abstract: Triangular silver nanoplates were prepared by using the seeding growth approach with the presence of citrate-stabilized silver seeds and a mixture of gelatin–chitosan as the protecting agent. By understanding the critical role of reaction components, the synthesis process was improved to prepare the triangular nanoplates with high yield and efficiency. Different morphologies of silver nanostructures, such as triangular nanoplates, hexagonal nanoprisms, or nanodisks, can be obtained by changing experimental parameters, including precursor $AgNO_3$ volume, gelatin–chitosan concentration ratios, and the pH conditions. The edge lengths of triangular silver nanoplates were successfully controlled, primarily through the addition of silver nitrate under appropriate condition. As-prepared triangular silver nanoplates were characterized by transmission electron microscopy (TEM), dynamic light scattering (DLS), UV-Vis, Fourier transform infrared spectroscopy (FT-IR), and X-Ray diffraction (XRD). Silver nanoplates had an average edge length of 65–80 nm depending on experimental conditions and exhibited a surface plasma resonance absorbance peak at 340, 450, and 700 nm. The specific interactions of gelatin and chitosan with triangular AgNPs were demonstrated by FT-IR. Based on the characterization, the growth mechanism of triangular silver nanoplates was theoretically proposed regarding the twinned crystal of the initial nanoparticle seeds and the crystal face-blocking role of the gelatin–chitosan mixture. Moreover, the antibacterial activity of triangular silver nanoplates was considerably improved in comparison with that of spherical shape when tested against Gram-positive and Gram-negative bacteria species, with 6.0 ug/mL of triangular silver nanoplates as the MBC (Minimum bactericidal concentration) for *Escherichia coli* and *Vibrio cholera*, and 8.0 ug/mL as the MBC for *Staphylococcus aureus* and *Pseudomonas aeruginosa*. The MIC (Minimum inhibitory concentration) of triangular Ag nanoplates was 4.0 ug/mL for *E. coli*, *V. cholera*, *S. aureus*, and *P. aeruginosa*.

Keywords: triangular silver nanoplates; antibacterial activity; gelatin; seeding growth approach

1. Introduction

Nanoscale materials have been extensively studied with respect to their potential applications and synthesis procedures [1–7]. Among the research areas, the modification of methods for controlled synthesis of triangular silver nanoplates has attracted a lot of attention in recent years due to the widespread application of silver nanoplates in various fields, such as surface-enhanced Raman scattering (SERS) detection or manufacture of antibacterial agents [8–13]. Due to the high anisotropy of sharp vertices and edges, triangular silver nanoplates can exhibit unique optical [14] and antimicrobial properties [12]. For example, due to the dependence of the bactericidal activity of silver nanoparticles on the free Ag^+ ions released from the Ag nanoparticles [15,16], it is possible to enhance the antibacterial performance by morphologically tuning spherical silver nanoparticles into triangular silver nanoplates that have three sharp tips. In addition, Qing et al. analyzed the antibacterial mechanisms through direct contact with microorganisms in their work [17]. The Ag nanoparticles could attach to the bacterial cell wall and penetrate through it. This process would cause membrane damage and consequently the cellular content leaks out, resulting in bacterial death [17–19]. Another antibacterial mechanism of Ag nanoparticles was described in several works, related to the generation of a high level of reactive oxygen species (ROS) and free radical species [20–22]. Furthermore, the surrounding media of AgNPs colloid is also related to their antibacterial activities. To be specific, it was found that the aggregation of silver nano in the environment with the electrolyte contents could reduce antibacterial properties [13,23]. Therefore, the controlling of both morphological growth and the ambient media of triangular AgNPs is critical to produce AgNPs with improved antibacterial behaviors.

Generally, the controlled synthesis of triangular AgNPs by the chemical reduction method follows two steps [24]: (i) the generation of small seed particles and (ii) the growth of triangular AgNPs in the presence of a capping agent under an appropriate condition. A variety of stabilizing agents and surfactants, such as cetyltrimethylammonium bromide (CTAB) [25,26], poly (N-vinyl-2-pyrrolidone) (PVP) [27], and a mixture of polyethylene glycol (PEG) and PVP [10], were used to synthesize the silver nanoplates. However, to the best of our knowledge, there are very few works using the mixed solutions of gelatin and chitosan as the stabilizing system in the synthesis of triangular AgNPs. The mixture of gelatin and chitosan could be an ideal candidate in the chemical reduction method due to several advantages, including easy adjustment of the environment viscosity [9,28,29], electrostatic repulsion [28], and the presence of capping ligands for the selective facets of particles [30]. To be specific, the use of a mixed solution as the stabilizing system permits effortless adjustment of the solution viscosity by varying the pH and ionic strength conditions [28], which in turn governs the growth process of triangular AgNPs. Furthermore, with the presence of chitosan as a cationic natural polymer, under a suitable pH value [31,32], the formed triangular AgNPs could effectively interact with the negatively charged membranes of organisms to release higher concentration of ion Ag^+, thereby improving the bactericidal properties of the formed nanoparticles. This mechanism was elaborated by the study of Sukdeb et al. where coagulation of nanoparticles, caused by the charge neutralized interaction, was proposed to bring about synergistic effects of silver nanoparticles and cationic protecting agent on negative charge cells [13]. On the other hand, chitosan has been previously reported as a potent antibacterial agent against Gram-positive and Gram-negative bacteria [33,34].

In this work, we developed a preparation route of triangular AgNPs based on the seed-mediated procedure. This is the first time the morphology conversion of silver nanoparticles from hexagonal to triangular plates has been achieved through changing the ratios of mixed gelatin–chitosan concentrations and experimental factors. Moreover, using the mixture of these two protein and polysaccharides instead of conventional surfactants could shed light on new applications of chitosan and gelatin in biological fields. In addition, antibacterial activities of the synthesized triangular AgNPs

were evaluated against various species of bacteria, including *Staphylococcus aureus*, *Escherichia coli*, *Vibrio cholerae*, and *Pseudomonas aeruginosa*.

2. Experimental

2.1. Materials

Silver nitrate ($AgNO_3$, 99.9%), trisodium citrate ($Na_3C_6H_5O_7.3H_2O$, 99.9%), H_2O_2 (30 wt-%), and sodium borohydride ($NaBH_4$, 99.9%) were obtained from Merck (Darmstadt, Germany) and used as received. Gelatin (Type B from porcine skin) was purchased from Sigma-Aldrich (Darmstadt, Germany). L (+)-Ascorbic acid ($C_6H_8O_6$ 99.9%) was purchased from Prolabo (Paris, France). *Escherichia coli* (American Type Culture Collection-ATCC 25922), *Staphylococcus aureus* (ATCC 25923), *Pseudomonas aeruginosa* (ATCC 9027), and *Vibrio cholera* (ATCC 15748) were obtained from the Thermo Fisher Scientific (Mumbai, India). Tryptone soya broth (TSB), tryptone soya agar (TSA), and peptone salt were purchased from HIMEDIA (Mumbai, India). Chloramphenicol (99.57%) was obtained from Calbiochem (Darmstadt, Germany). All chemical reagents and solvents used in this work were of analytical grade and aqueous solutions were prepared using deionized water (conductivity was below 4.3 μS/cm).

2.2. Preparation of Silver Seeds

The silver seeds were prepared using the sodium borohydride as reducing agent, according to a previous report [35]. In a typical procedure, 20 mL aqueous solution of $AgNO_3$ 3.0×10^{-4} M was mixed with 20 mL of trisodium citrate (TSC) 5.0×10^{-4} M, and then cooled in an ice-bath. Subsequently, 60 μL solution of $NaBH_4$ (0.1 M) was slowly added to the mixture under vigorous stirring, resulting in the generation of silver seeds with a bright yellow colloidal solution. In order to avoid photo-degradation, the silver seeds colloid was preserved from the light for 3 h before use.

2.3. Growth of Triangular Silver Nanoplates

Gelatin solutions (0.05–0.5%, *w*/*v*) were obtained by swelling an amount of gelatin powder in deionized water (<4.3 μS/cm) for 20 min at room temperature, followed by stirring at 500 rpm at 60 °C for 30 min. Chitosan (CHI) solutions (0.06%, *w*/*v*) were prepared by dissolving CHI powder into an aqueous solution of acetic acid (1.0%, *v*/*v*), followed by stirring at 700 rpm for 7 h at room temperature. Mixtures of different gelatin concentrations (0.05–0.5%, *w*/*v*) with a fixed CHI concentration of 0.06% (*w*/*v*) were prepared by combining equal volumes of gelatin and chitosan, and stirring the mixture at 500 rpm for 45 min. A certain amount of HCl (1.0 M) or NaOH (1.0 M) solution was used to adjust the pH values of the gelatin–chitosan mixtures.

Triangular silver nanoplates (AgNPs) were synthesized with the preformed Ag seeds. In a typical sample, a 200 μL volume of silver seeds colloid was combined with the 6.0 mL mixture of gelatin (0.2%, *w*/*v*)-chitosan (0.06%, *w*/*v*), H_2O_2 (50 μL, 30 wt-%), and ascorbic acid (40 μL, 0.1 M) solution. Finally, $AgNO_3$ (175 μL, 0.01 M) was then slowly added into the above mixture, followed by stirring at 700 rpm at room temperature. The color of the colloidal dispersion changed from transparent to yellow, orange, blue, and finally to dark green, indicating the formation of nanoplates in the colloidal solution. The total volume of 10 mL was adjusted by adding deionized (DI) water.

2.4. Microorganism Preparation

Escherichia coli, *Staphylococcus aureus*, *Pseudomonas aeruginosa*, and *Vibrio cholera* were cultivated in TSB at 35 °C for 24 h. The culture suspensions were then diluted with sterile Tryptone soy broth, estimated to 10^8 CFU.mL^{-1} by correlation between optical density at 600 nm and cells number. The standard curves were established for each bateria based on Keiran Stevenson's method [36].

2.5. Antibacterial Activity Test

For evaluating the susceptibility of bacteria to the silver nanoparticles, based on the modified Kirby–Bauer method [36–38], paper discs with a diameter of 5 mm were immersed in different concentrations of Ag nanoplates colloids (from 0 to 50 ppm) before being placed onto the agar plates, which had been seeded with the microorganisms earlier. In order to be used as the negative control, the other paper disc containing no sample was also prepared. Subsequently, the inhibition zones were evaluated visually after incubating for 24 h.

The MIC (minimum inhibitory concentration) of triangular Ag nanoplates against the four bacteria species was recorded as the lowest concentration required to inhibit the growth of the initial amount of bacteria [39]. The minimal bactericidal concentration (MBC) is the lowest concentration of an antibacterial agent required to kill completely the initial amount of bacteria. The MBC represents the bacteria death, whereas the MIC gives information about the multiplication stoped [39]. In a typical experiment, a 200 μL sample of bacterial suspension (10^8 CFU/mL) was inoculated into flasks containing 20 mL of TSB, treated with various concentrations of AgNPs (0, 2, 4, 6, 8, 10, 12 μg/mL). The as-prepared flasks were incubated further at 35 °C for 16 h and continuously agitated by placing on an orbital shaker in the dark room. After incubating, microbial densities were determined with pour plate technique [40], using peptone salt water as dilution broth and TSA as solid culture medium. The plates were then incubated at 35 °C for 16 h. All resultant colonies were examined by counting the surviving bacterial cells on the plate, and each sample was repeated in triplicate. The MIC was reported as the average value of the three independent measurements.

2.6. Characterization

UV-Vis spectra were obtained by using a UV-Vis-NIR-V670 spectrophotometer (JASCO, Japan). The samples were measured with a scanning rate of 200 nm per minute between 300 and 800 nm, using 1-cm path length quartz cuvettes. The X-Ray diffraction (XRD) patterns were performed by using a D8 Advance-Bruker, Germany, equipped with Cu-K radiation at scanning rate of 4° per minute in the 2θ range from 30° to 80° (40 kV, 40 mA). The morphologies and size of AgNPs were determined by transmission electron microscopy (TEM) (JEM-1400, Japan). The sample was prepared by placing a drop of colloid on a carbon copper grid (300-mesh, Ted Pella, Inc., USA) and subsequently being air-dried for 15 min. The size distributions and average sizes of AgNPs were characterized by the dynamic light scattering (DLS) technique using SZ-100 (Horiba, Japan). Zeta potential values of triangular AgNPs colloidal dispersion were also determined with SZ-100 (Horiba, Japan).

3. Results and Discussion

3.1. Effect of Silver Nitrate

The preparation of silver seeds was carried out by using $NaBH_4$ as a reducing agent and TSC as a stabilizer, resulting in the formation of a number of seed particles with an average size of 6.22 nm (Figure 1a,b). The initial seeds were previously demonstrated as a critical factor for the formation of different morphologies of AgNPs, preceding elements of appropriate surfactant and synthetic conditions [16].

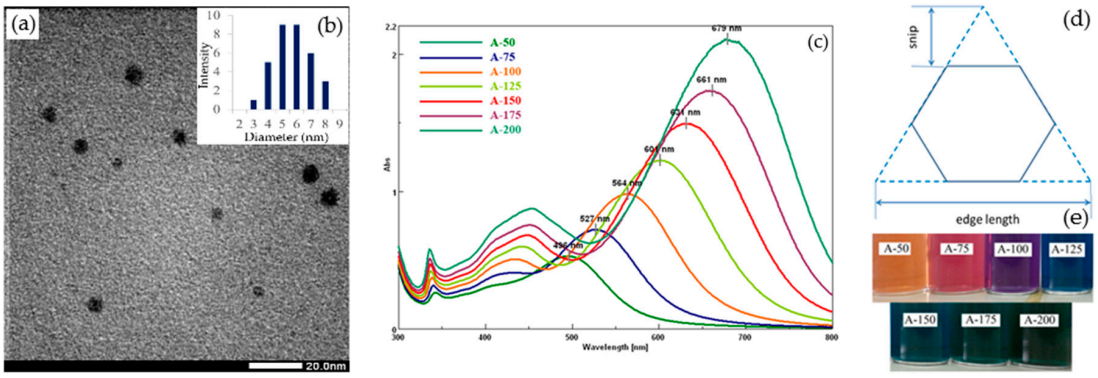

Figure 1. (**a**) Transmission electron microscopy (TEM) images of the initial silver seeds (20 mL $AgNO_3$ 3.0×10^{-4} M, 20 mL of TSC 5.0×10^{-4} M, 60 µL solution of $NaBH_4$ 0.1 M), (**b**) the inset of the size distribution of formed seeds (measured by TEM), (**c**) UV-Vis spectra of triangular AgNPs synthesized by different volumes (from 50 to 200 µL) of $AgNO_3$ 0.01 M, 6.0 mL mixed solution of gelatin (0.2%, *w*/*v*)-chitosan (0.06%, *w*/*v*), (**d**) the inset of the snipped tips and edge length of a silver nanoplate theme, and (**e**) digital photographs of the samples at different volumes of $AgNO_3$ 0.01 M (range from 50 to 200 µL).

The formation of triangular AgNPs in colloidal dispersion can be identified through the appearance of the surface plasmon resonance (SPR) peaks at the positions of about 340, 450, and 650 nm, which attributed to the out-of-plane quadrupole, in-plane quadrupole, and in-plane dipole resonances of triangular silver nanoplates, respectively [16,41]. It was noted that the quadrupole plasmon resonances of the nanoplates could only be observed with adequately high concentrations of formed nanoplates, corresponding to the narrow size and shape distributions in the colloidal dispersion [41,42]. Additionally, the absorption peaks attributed to the multipole resonances were also dependent on the dimension of triangular silver, including edge length and thickness of nanoplates [18,31,33]. In this regard, Kevin et al. previously defined an aspect ratio (AR) as the edge length divided by the thickness of nanoplates [42].

The UV-Vis results implied that, as the volume of $AgNO_3$ 0.01 M decreased from 200 to 50 µL, the SPR peaks of silver nanoplates became blue-shifted (from 670 to 496 nm). This blue-shift in optical features can be related to the sharper vertices of triangular AgNPs, which was previously explained due to the change of the electron cloud density on the nanoparticles surface [14]. In the growth process of triangular AgNPs, silver nitrate can provide Ag^o atoms through the reduction of Ag^+ ions induced by ascorbic acid. Therefore, the use of $AgNO_3$ in a sufficient quantity, in conjunction with an appropriate ratio of mixed gelatin–chitosan solution, could be the key for adjusting the diffusion rate of Ag^o atom, which allowed us to control the edges length and vertices of triangular AgNPs. For instance, at the low initial volume of $AgNO_3$, the peaks at 527 and 434 nm (observed in the UV-Vis spectrum of the A-75 sample, 75 µL $AgNO_3$ 0.01 M), featured for the formation of disk-like morphologies [24], showed remarkable shifts to 679 and 453 nm, respectively (Figure 1 curve A-200) (the sample of 200 µL $AgNO_3$ 0.01 M), when increasing the volume of $AgNO_3$ 0.01 M to 200 µL. According to previous reports [42], this change indicates the conversion to the triangular AgNPs with an approximate AR of 2.5.

Consistent with UV-Vis results, different shapes of AgNPs (such as disk-like, hexagonal, and truncated-plates nanostructures) were observed in TEM images of sample A-75 (75 µL $AgNO_3$ 0.01 M) (Figure 2a), showing a broad size distribution (measured by TEM). Additionally, hexagonal silver nanoplates with an extensive growth in edge length to about 40–46 nm were further obtained when increased the volume of $AgNO_3$ (0.01 M) to 125 µL (Figure 2b). From the preliminary results, it is suggested that an evolution from hexagonal to triangular shape could be achieved by increasing the volume of $AgNO_3$ 0.01 M to 200 µL (Figure 2c). However, the growth of triangular AgNPs could also be conditional on the diffusion rate of Ag^+ ions to the initial seeds growth surfaces [12,24]. Thus, the controlled synthesis of triangular AgNPs was apparently related not only to the crystal

growth of the silver seeds induced by Ag^+ ion [24,43], but also to the suppressing roles of the mixed gelatin–chitosan solution.

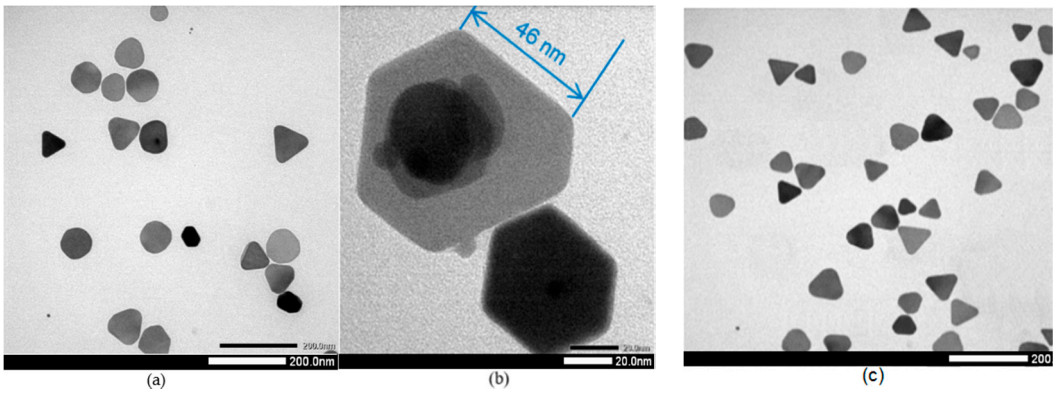

Figure 2. TEM images of (**a**) the nanodisk shapes (scale 200 nm) (75 μL $AgNO_3$ 0.01 M); (**b**) the hexagonal shapes (scale 20 nm) (125 μL $AgNO_3$ 0.01 M); and (**c**) high yield of triangular shapes (80%) of silver nanoplates (200 μL $AgNO_3$ 0.01 M) (scale 200 nm).

3.2. *Effect of Mixed Gelatin–Chitosan Solution*

In the growth process, the silver nanoplate fusion rate can be controlled by the regulation of environment viscosity, which is closely related to the complexation process of the two protein-polysaccharide polymers under the appropriate conditions (such as composition ratio and the pH values) [28,44].

To further clarify the role of the mixed solution, the growth process of silver nanoplates was carried out in the absence of the gelatin–chitosan mixture. In the spectrum of AgNPs synthesized without gelatin and chitosan (Figure 3, Table 1), only two absorbance peaks located at 488 and 342 nm could be observed, indicating that the quasi-spherical and spherical morphologies could be formed in the colloidal solution. As the concentration of gelatin increased from zero to 0.2% (*w*/*v*), the plasmon peak assigned to the in-plane dipole resonance of AgNPs was red-shifted from 488 to 663 nm (Figure 1, Table 1). The intensity of plasmon peak located at 663 nm increased significantly to 1.89, which might be attributed to the extension of sharper vertices of AgNPs. However, when increasing the gelatin concentration to 0.5% (*w*/*v*), the SPR peak was reversely blue-shifted to the wavelength 638 nm and the intensity of this peak was also decreased to 1.48 (Table 1). This blue-shifting clearly indicates the transformation of particle shape from triangular to other morphologies (such as truncated, disk-like, and hexagonal).

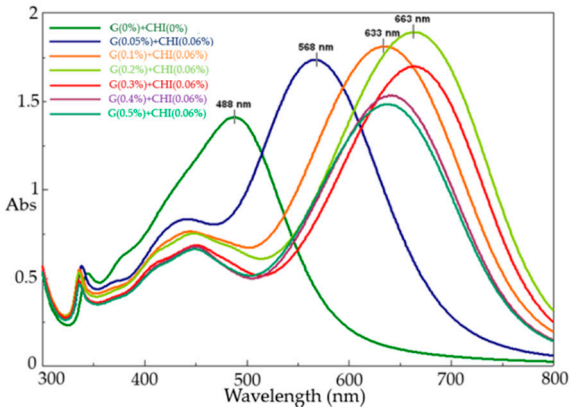

Figure 3. UV-Vis spectra of triangular AgNPs synthesized by different concentrations ratios of mixed gelatin (type B)–chitosan (from 0–0.06 to 3.0–0.06, *w*/*v*).

Table 1. UV-Vis results of triangular Ag nanoplates synthesized by different concentration ratios of gelatin–chitosan mixture.

Sample	Peak 1		Peak 2		Peak 3	
	λ_{max} (nm)	Abs	λ_{max} (nm)	Abs	λ_{max} (nm)	Abs
G(0%) + CHI(0%)	342	0.525	-	-	488	1.40
G(0.05%) + CHI(0.06%)	342	0.566	441	0.832	568	1.73
G(0.1%) + CHI(0.06%)	336	0.547	445	0.761	633	1.81
G(0.2%) + CHI(0.06%)	335	0.530	449	0.751	663	1.89
G(0.3%) + CHI(0.06%)	335	0.485	451	0.684	664	1.70
G(0.4%) + CHI(0.06%)	336	0.470	450	0.676	639	1.53
G(0.5%) + CHI(0.06%)	336	0.465	450	0.661	638	1.48

This conversion phenomena could be explained based on the electrostatic repulsion in the dispersion that was caused by the charge density of two biopolymers [45]. When gelatin concentration increased, the charge density also increased, leading to the promotion of electrostatic repulsion and in turn accelerated mobility of growth species. As a result, other random fusions are more likely to occur and the disk-liked or hexagonal nanoplates would be formed naturally.

Corresponding to the UV-Vis data, the conversion from quasi-spherical to triangular and hexagonal shapes of AgNPs was clearly observed in the TEM image (Figure 4a,b). Moreover, at the G + CHI concentration of 0.2 + 0.06% (*w*/*v*), a relatively high yield of triangular AgNPs (70%) with the sharp vertices was achieved (Figure 4c). It was previously suggested that gelatin selectively bound to the {111} crystalline facets through the thiol and amine groups [30]. With a sufficient concentration of gelatin, we hypothesize that these polymer molecules can only cover the {111} lattice planes at the top and bottom large surfaces of twinned-crystal because of low steric hindrance. This inhibits the adsorption of Ag^{o} atom onto these surfaces, and thereby allows extensive growth along the grooves of twinned crystal seeds, resulting in the formation of triangular silver nanoplates. Additionally, according to representative studies on gelatin and chitosan [44,45], higher gelatin concentration was suggested to cause the gelation process [46,47], and thus the gelatin conformation would be changed from stretching random coils to triple-helix form [29,46]. This process could reduce the adsorption of gelatin molecules onto favorable surfaces, resulting in the overgrowth of different morphologies of nanoparticles in the colloidal dispersion.

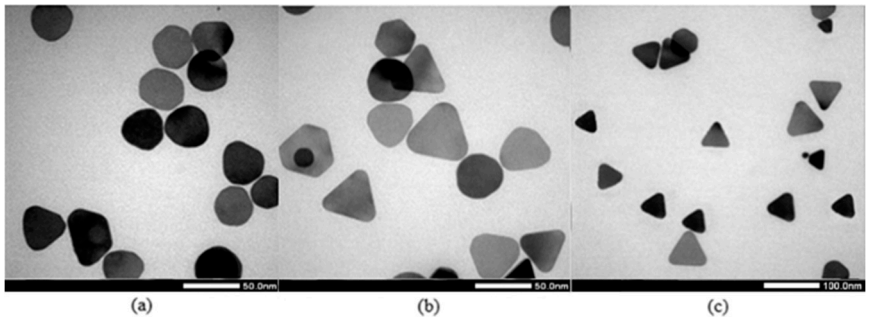

Figure 4. TEM images of (**a**) nano disk shapes (scale 50 nm) (G + CHI 0%, *w*/*v*); (**b**) hexagonal (30%) and triangular shapes (50%) (scale 50 nm) (G + CHI 0.5 + 0.06%, *w*/*v*); and (**c**) high yield of triangular shapes of AgNPs (70%) (scale 100 nm) (G + CHI 0.2 + 0.06%).

The advantage of using chitosan is to enhance the stability of triangular AgNPs under the ionic strength condition. In order to clarify the effect of chitosan, various samples of AgNPs colloids were prepared with or without the presence of chitosan (0.06%, *w*/*v*), with the addition of NaCl 1.0 M aqueous solution. In the absence of chitosan, the three characteristic peaks of triangular morphology located at 588, 439, 337 nm could also be observed in the spectrum of AgNPs colloidal dispersion (Figure 5A

curve b). However, after adding the solution of NaCl 1.0 M, the intensity of these peaks dropped dramatically (Figure 5A curve d), suggesting that the self-aggregation induced by the electrostatic repulsion was possibly linked to the reduced number of formed triangular AgNPs in the dispersion. In the case of using chitosan, as shown in Figure 5A (curve a), the intensity of characteristic peak at 667 nm slightly decreased from 1.48 to 1.23 (curve c), indicating the formation of triangular AgNPs was relatively well-preserved. The UV-Vis results thus support the view that chitosan could prevent the triangular AgNPs from the influence of ionic forces in the colloidal dispersion. This protecting effect might come from the neutralized interaction between the Cl^- anion and the glucosamine units of chitosan through the amine and hydroxyl groups. It is worth noting that chitosan stays as its positive charged form in the pH value range from 3.0 to 9.0 [28,45]. For this reason, the electrostatic repulsion of ions can be effectively decreased to contribute to stabilizing the formation of triangular AgNPs.

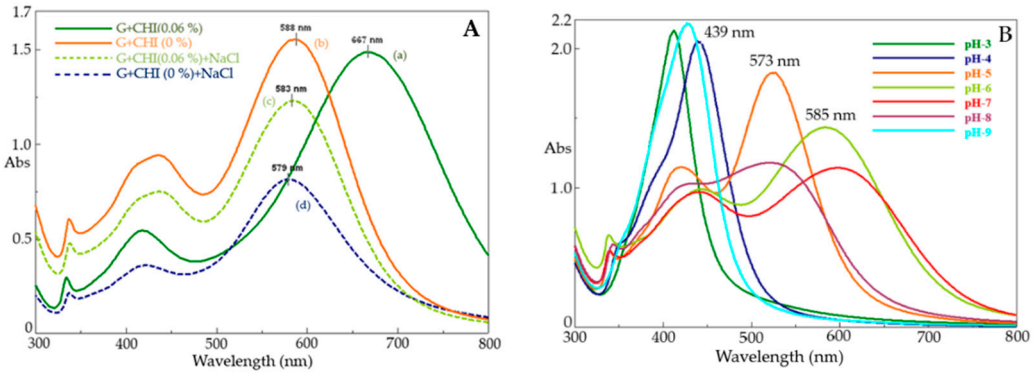

Figure 5. (**A**) UV-Vis spectra of triangular AgNPs colloidal dispersions synthesized with chitosan 0.06% (*w*/*v*) (gelatin 0.2%, *w*/*v*) (curve a), without chitosan (gelatin 0.2%, *w*/*v*) (curve b), with the presence of chitosan 0.06% after adding NaCl 1.0 M (curve c), and without chitosan after adding NaCl 1.0 M (curve d). (**B**) UV-Vis spectra of triangular AgNPs synthesized at different pH values (from 3.0 to 9.0) with gelatin (0.2%, *w*/*v*)-chitosan (0.06%, *w*/*v*).

3.3. Effect of pH Condition

To further investigate the effect of the pH values, the synthesis of triangular AgNPs was carried out at seven pH values ranging from 3.0 to 9.0. As shown in the Figure 5B, the three characteristic peaks of triangular plates located at 338, 444, and 585 nm were clearly observed in the spectrum of the sample prepared at pH 6.0 (Figure 5B, Table 2), implying the formation of triangular AgNPs. As pH value dropped to below 5.0, only one plasmon peak at 439 nm featured for the spherical morphology of silver nanoparticles could be seen on the UV-Vis spectrum of the sample prepared at pH 4.0 (Figure 5, Table 2). Similar results were also obtained when carried out at pH 3.0 and 9.0. The UV-Vis data thus reveal the critical role of pH on the mixture of gelatin and chitosan, which directly controls the growth of triangular AgNPs. It should be noted that at pH values below the isoelectric point (pI 5.0), gelatin (type B) exists as positive charge forms [28,45], which, in conjunction with the positive charge of chitosan, could lead to the increase in repulsion between the growth species. Consequently, the random growth process was more likely, and the irregular shapes were preferentially formed. At pH values of 5.0–7.0, the negative charge forms of gelatin took place and interacted with the positive charge forms of chitosan [29,45], followed by the decrease in repulsion forces because of charge neutralization. In this case, the diffusion rate of Ag^o atom to the favorable surface of twinned-crystal seeds can be controlled and the triangular AgNPs growth process will be further promoted. Besides this, when the interaction of two polymers was formed, the viscosity of the colloidal solution was subsequently increased [28]. This is another possible reason that explains the constrained mobility of the Ag^o atom, resulting in the formation of triangular AgNPs.

Table 2. UV-Vis results of triangular Ag nanoplates synthesized by a mixture of gelatin (0.2%, *w*/*v*)-chitosan (0.06%, *w*/*v*) at different pH values.

Sample	Peak 1		Peak 2		Peak 3	
	λ_{max} (nm)	Abs	λ_{max} (nm)	Abs	λ_{max} (nm)	Abs
pH 3.0	412	2.12	-	-	-	-
pH 4.0	439	2.04	-	-	-	-
pH 5.0	337	0.500	435	0.770	573	1.72
pH 6.0	338	0.660	444	0.988	585	1.42
pH 7.0	339	0.545	441	0.968	598	1.14
pH 8.0	341	0.581	-	-	522	1.17
pH 9.0	427	2.17	-	-	-	-

Corresponding to the UV-Vis observation, TEM images (Figure 6a) showed that the spherical and quasi-spherical shapes appeared at pH below 5.0, and the average size of AgNPs, measured by TEM, was 82.5 nm. Various shapes of silver nanoparticles were also obtained as the pH values were increased to 8.0–9.0 (Figure 6c). In both cases, the average size of the nanoparticles was above 100 nm, characterized by the DLS method (Figure 7a–c). These results are slightly different from the average size measured by TEM and could be explained by the stabilizing layers on the surface of AgNPs. However, the formation of triangular silver nanoplates did take place at the pH value of 6.0 with an average edge size of 54.5 nm, measured by TEM (Figure 6b). From DLS data, the average size of AgNPs was about 74.6 nm (Figure 7b), and the size distribution was relatively narrow.

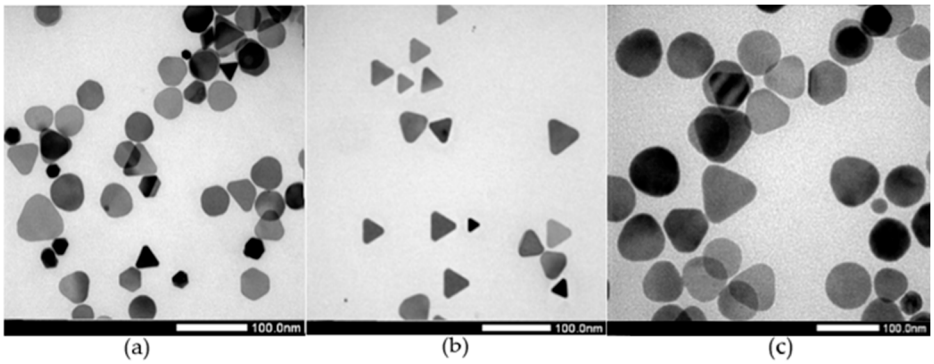

Figure 6. TEM images of silver nanoparticles synthesized mixed gelatin (0.2%, *w*/*v*)-chitosan (0.06%, *w*/*v*) solution at (**a**) pH 4.0, (**b**) pH 6.0, and (**c**) pH 8.0 (scale 100 nm).

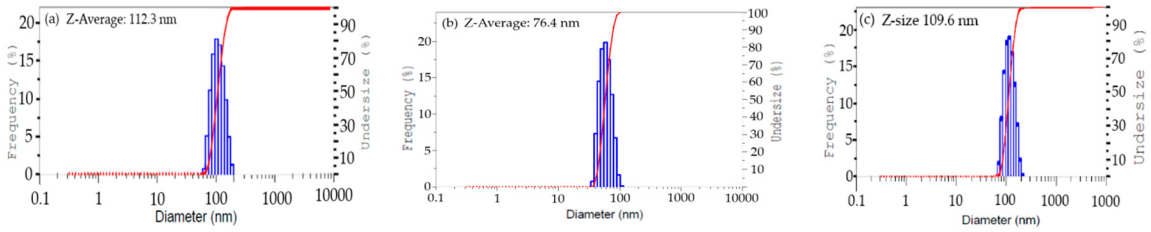

Figure 7. Dynamic Light Scattering (DLS) results of silver nanoparticles prepared by mixed gelatin (0.2%, *w*/*v*)-chitosan (0.06%, *w*/*v*) solution at (**a**) pH 4.0, (**b**) pH 6.0, and (**c**) pH 8.0.

3.4. X-ray Diffraction Analysis of Silver Nanoparticles

The crystalline structure of triangular silver nanoplates was characterized with XRD patterns (Figure 8). The highest intensity diffraction peak was observed at 2θ = 38.101°, assigned to the {111} facets, clarifying the extensive growth of the {111} lattice plane to form the triangular AgNPs. Lower intensity diffraction peaks located at 44.34° and 65.5° were attributed to the {200} and {220} planes of

face-center cubic (fcc), respectively. This XRD results are further commensurate with previous studies on the triangular and disk-like morphologies [13,26], where only diffraction peaks attributed to the {111} lattice planes could be remarkably observed.

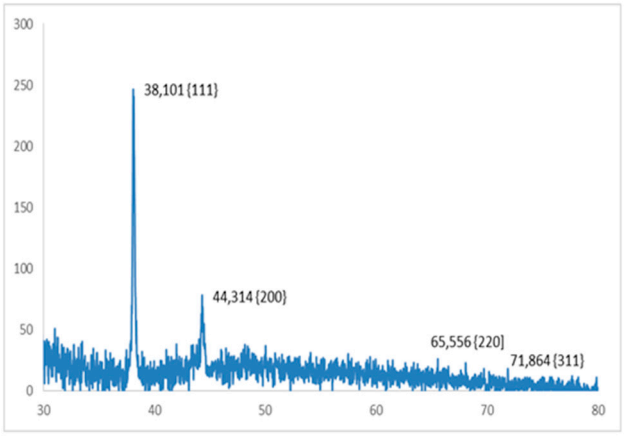

Figure 8. XRD pattern of triangular silver nanoplates stabilized by the mixture of gelatin 0.2 (%, *w*/*v*) and chitosan 0.06 (%, *w*/*v*) at pH 6.0.

3.5. FTIR Analysis of Gelatin–Chitosan-Triangular AgNPs Interaction

The specific interaction of gelatin–chitosan with AgNPs were characterized by FT-IR spectroscopy (Figure 9 and Table 3). The typical FT-IR spectrum of pure gelatin (curve b) showed the characteristic bands located at 1650 cm^{-1} that were assigned to the amide I group (C=O stretching vibration) and the bands at 1540 cm^{-1} attributed to the N–H vibration in amide II groups [48]. It was observed that the intensity of these bands decreased dramatically in the spectrum of triangular AgNPs synthesized by the gelatin–chitosan mixture (Figure 9 curve c). The bands located at 1650 cm^{-1} and 1540 cm^{-1} also shifted to 1643 cm^{-1} and 1547 cm^{-1}, respectively (Figure 9 curve c). Moreover, the bands in the 1400–1500 cm^{-1} region mainly represented to the COO- symmetrical stretching vibrations [48]. In the case of interaction with triangular AgNPs, these bands' intensities were found to decrease remarkably (Figure 9 curve c). The presence of bands from 3447 to 2991 cm^{-1} in the spectrum of gelatin–chitosan-triangular AgNPS (Figure 9 curve c) was assigned to the $–NH_2$, –OH, and $–CH_2$, and $–CH_3$ aliphatic groups in the chitosan molecules [49]. These bands' intensities were lower than the corresponding absorbance bands observed in the spectrum of pure chitosan (Figure 9 curve a), suggesting the interaction between triangular AgNPs and chitosan. Consequently, the FT-IR results revealed that the gelatin and chitosan molecules could interact specifically with the triangular AgNPs through the functional groups (i.e., $–NH_2$, –OH, COO-, and $–CO–NH_2$).

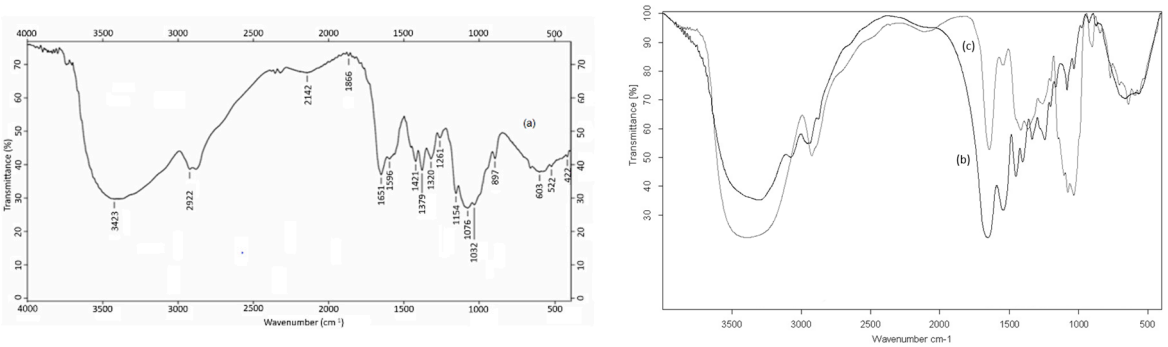

Figure 9. FT-IR spectra of pure chitosan (curve a), pure gelatin (curve b) and gelatin–chitosan-AuNPs (mixture of gelatin 0.2 (%, *w*/*v*) and chitosan 0.06 (%, *w*/*v*) at pH 6.0 (curve c).

Table 3. FT-IR band positions of pure gelatin, pure chitosan, and gelatin–chitosan mixture-AgNPs presented in Figure 9.

Position (cm^{-1}) Pure Chitosan (Curve b)	Position (cm^{-1}) Pure Gelatin (Curve b)	Position (cm^{-1}) Gelatin–chitosan-AgNPs (Curve c)	Assignment
3447–2991		3447–2991	$–NH_2$, –OH, $–CH_2$, $–CH_3$ aliphatic group
	3393	3304	Hydrogen bonds of retain water
1657			$–CONH_2$ group of chitosan
	1650	1643	Amide I (C=O stretching vibration)
	1540	1547	Amide II (N–H bending vibration)
	1400–1500		COO– symmetrical stretching vibration
1422			–OH group of the primary alcoholic group

3.6. Proposed Mechanism of Triangular AgNPs

Based on the previous studies [12,24,41], it is believed that the formation of triangular AgNPs is intimately related to the twinned-crystal seeds and kinetic control. Besides this, the presence of stabilizing agents has been proven to be a key factor in the growth of AgNPs that could promote the face-blocking process through the selective interaction. Moreover, adequately high gelatin concentration and volume of $AgNO_3$ can achieve a high yield of triangular silver nanoplates. This phenomenon may be due to the increased likelihood of initial seeds to stack, which results in the formation of twinned crystals. This speculation seems to be in line with the previous experiment of Antoniades and Wey on AgBr seeds [50]. In the subsequent growth step where the stacking faults of twinned crystals were formed, controlling the diffusion rate of Ag^o atom to the concave {111} facets as well as the appropriate addition of $AgNO_3$ precursor could be effective ways to obtain the triangular shape. By using the mixed solution of chitosan and gelatin, the generation rate and the mobility of Ag^o could be slowed down based on the regulation of viscosity and electrostatic repulsion at an appropriate pH condition.

3.7. Antibacterial Assay

The antibacterial activity of triangular silver nanoplates and the gelatin–chitosan mixture was examined with various strains of bacteria, including *E. coli*, *S. aureus*, *V. cholera*, and *P. aeruginosa*. We investigated the antibacterial performance with respect to the varying concentrations of mixed polymers and triangular silver nanoplates colloid. This differentiates our assays from previous studies, where the effects of silver nanoparticle dimension [12,13] and the polymers on the antibacterial properties were described [23]. The antibacterial properties of triangular AgNPs colloid may be due to the released Ag^+ ion capability from the sharp vertices of Ag nanoplates and the high interaction probabilities of polymers with the bacteria membranes.

In the disk diffusion method (Figure 10), the inhibition zones were used to evaluate the susceptibility of four bacteria species to the triangular AgNPs colloids. As shown in Figure 10, clear zones were visually observed around the disks which were treated with triangular AgNPs. This demonstrated that the triangular AgNPs colloid (concentration 50 μg/mL) had bactericidal capability against these Gram-negative and Gram-positive species. In particular, the significant inhibitions against *P. aeruginosa* and *S. aureus* were exhibited by triangular AgNPs colloids (A1, A2 samples at pH values of 6.0 and 5.0, respectively) synthesized by the mixed gelatin–chitosan solution, whereas the chloramphenicol antibiotic (sample C) (100 μg/mL) exerted almost no effect on them. On the contrary, triangular AgNPs still gave very clear inhibition results (Figure 10A–D).

In order to clarify the role of silver nanoparticles dimension in antibacterial performance, a comparative experiment was carried out with the sample of spherical AgNPs under the identical concentration. Figure 10E–H showed the inhibition zones of the plates treated with the sample A3 (spherical AgNPs 50 μg/mL synthesized by gelatin 0.2%, *w/v* at pH 3.0) and the sample A4 (spherical

AgNPs 50 μg/mL synthesized without the mixed gelatin chitosan solution). The spherical AgNPs samples (A3–A4) had smaller inhibition zones at the concentration of 50 μg/mL than the triangular AgNPs sample (A1) at the same concentration (Figure 10E–H). Overall, the results clearly indicate that the antibacterial activity of triangular AgNPs is better than spherical silver nanoparticles.

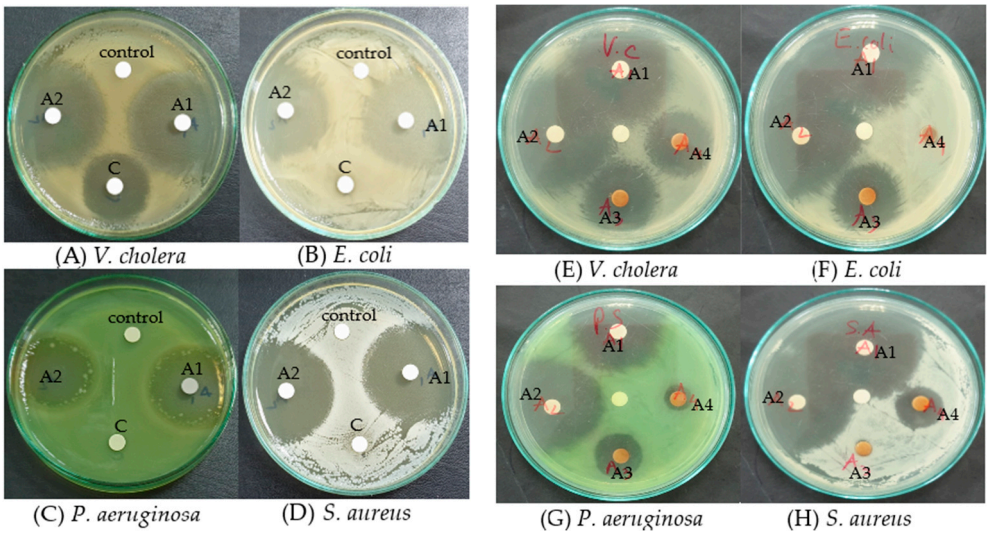

Figure 10. Inhibition zones of (**A**) *V. cholera*, (**B**) *E. coli*, (**C**) *P. aeruginosa,* and (**D**) *S. aureus* treated with A1 sample (triangular AgNPs 50 μg/mL synthesized by mixed G(0.2%) + CHI(0.06%) solution at pH 6.0), A2 sample (triangular AgNPs 50 μg/mL synthesized by mixed G(0.2%) + CHI(0.06%) solution at pH 5.0), C sample (chloramphenicol 100 μg/mL), and negative control sample. (**E**) *V. cholera*, (**F**) *E. coli*, (**G**) *P.aeruginosa,* and (**H**) *S. aureus* treated with the A3 sample (spherical AgNPs 50 μg/mL synthesized by G (0.2%) at pH 3.0), A4 sample (spherical AgNPs 50 μg/mL synthesized without mixed G + CHI solution).

For quantitative evaluation of the antibacterial activity, the MIC and MBC values were further examined through the testing experiments against *E. coli*, *S. aureus*, *P. aeruginosa*, and *V. cholera* at different concentrations of AgNPs (from 2 to 12 μg/mL). In the case of *E. coli* and *V. cholera*, the MBC value of triangular AgNPs was 6.0 μg/mL. The obtained MBC for both *S. aureus* and *P. aeruginosa* was 8.0 μg/mL (Figure 11). The MIC values of triangular AgNPs were 4.0 μg/mL for *E. coli*, *S. aureus*, *P. aeruginosa*, and *V. cholerae*, suggesting a smaller MIC value of triangular AgNPs in comparison with those of previous works of Weiwei Lu et al. [12] and Sukdeb Pal et al. [13].

Moreover, the high antibacterial activity of triangular AgNPs could be related to the {111} facet of the Ag crystalline structure, which was previously reported in the Morones et al. [51]. It was suggested that the bacterial cells could interact directly with the {111} facet of nanoparticles [13,51], resulting in transportation through the cell membrane of Ag^+ ion, and then cell death [13]. Because the spherical nanoparticles contain fewer {111} lattice planes than the triangular AgNPs, the binding of spherical nanoparticles thus seems to be lower than the triangular nanoplates. The anti-bacterial activities of released Ag^+ ions could be possibly explained based on various mechanisms. For intance, it was previously found that the Ag^+ ion caused the proton leakage through the *V. cholera* membrane, thus leading to the de-ernergization of the membrane [36]. Ag^+ ions strongly reacted with the –SH groups of the biomolecules and consequently inactivated several functions in the bacterial cells [47,48]. Furthermore, the bactericidal activity of the Ag^+ ion is possibly due to the prevention of DNA replication ability and the interference of adenosine triphosphate (ATP) production [48–50]. Ag^+ ions interacted with the enzyme NaDH dehydrogenase, leading to the uncoupling of respiration from ATP synthesis [50]. Besides this, Ag^+ ions moving inside the cell could generate reactive oxygen species (ROS) through readox reactions [52].

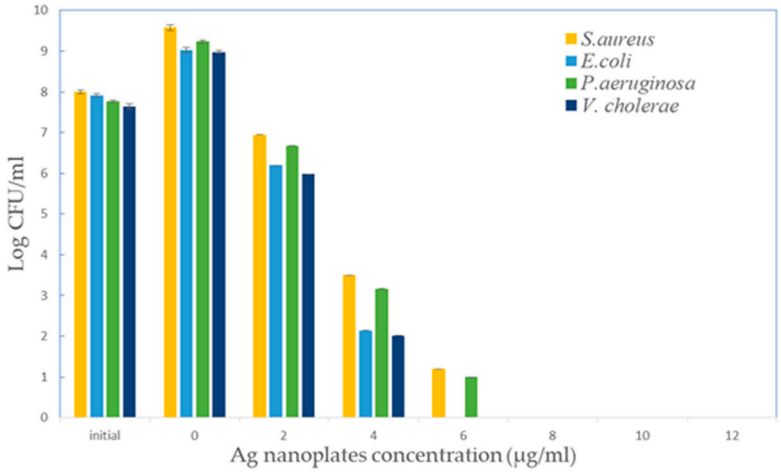

Figure 11. Growth inhibiton against *S. aureus*, *E. coli*, *P. aeruginosa*, and *V. cholera* supplemented with different concentrations of triangular silver nanoplates (from 2 to 12 μg/mL).

4. Conclusions

In summary, triangular silver nanoplates with an edge length of 46 nm were synthesized by a mixed solution of gelatin and chitosan based on the seed-mediated method. Current results indicated that using a mixed solution could further control the fusion rate of silver nanoplates to achieve a high yield of triangular AgNPs. The mechanisms for the nanoplate formation could be proposed on the basis of twinned crystal seeds and the face-blocking role of polymers. Furthermore, the influence of the particle morphologies on the antibacterial performance was also investigated. In comparison to spherical silver nanoparticles, triangular silver nanoparticles exhibited higher antibacterial activity. This could be due to the high anisotropic of the sharp vertices, which primarily account for the released of the Ag^+ ion and the efficient interaction to the bacteria cell membrane of the nanoparticles covered by gelatin and chitosan. From the results, it was found that mixed gelatin and chitosan showed high feasibility in the controlled synthesis of other morphologies of silver nanoparticles. This work would be favorable for further application in biological fields because of the high stability under the salt condition.

Author Contributions: Investigation, Q.K.V., D.D.P., Q.N.V.N., H.H.T., N.H.N.T., P.P.N.T., L.G.B. and L.V.T.; Writing—original draft, Q.K.V.

Funding: This research received no external funding.

Conflicts of Interest: The authors declare no conflict of interest.

References

1. Bach, L.G.; Islam, M.R.; Cao, X.T.; Park, J.M.; Lim, K.T. A novel photoluminescent nanohybrid of poly(ε-caprolactone) grafted Mg/Al layered double hydroxides and Tb3+ ions: Synthesis and characterization. *J. Alloys Compd.* **2014**, *582*, 22–28. [CrossRef]
2. Tanasa, E.; Zaharia, C.; Radu, I.-C.; Surdu, V.-A.; Vasile, B.S.; Damian, C.-M.; Andronescu, E. Novel Nanocomposites Based on Functionalized Magnetic Nanoparticles and Polyacrylamide: Preparation and Complex Characterization. *Nanomaterials* **2019**, *9*, 1384. [CrossRef] [PubMed]
3. Andronescu, E.; Predoi, D.; Neacsu, I.A.; Paduraru, A.V.; Musuc, A.M.; Trusca, R.; Oprea, O.; Tanasa, E.; Vasile, O.R.; Nicoara, A.I.; et al. Photoluminescent Hydroxylapatite: Eu3+ Doping Effect on Biological Behaviour. *Nanomaterials* **2019**, *9*, 1187. [CrossRef] [PubMed]
4. Lee, K.-W.; Kim, Y.-H.; Du, W.X.; Kim, J.-Y. Stretchable and Low-Haze Ag-Nanowire-Network 2-D Films Embedded into a Cross-linked Polydimethylsiloxane Elastomer. *Nanomaterials* **2019**, *9*, 576. [CrossRef]

5. Cernea, M.; Vasile, B.S.; Surdu, V.A.; Trusca, R.; Bartha, C.; Craciun, F.; Galassi, C. Probing the dielectric, piezoelectric and magnetic behavior of $CoFe_2O_4$/BNT-BT 0.08 composite thin film fabricated by sol-gel and spin-coating methods. *Sci. Rep.* **2018**, *8*, 17883. [CrossRef]
6. Islam, M.R.; Bach, L.G.; Nga, T.T.; Lim, K.T. Covalent ligation of gold coated iron nanoparticles to the multi-walled carbon nanotubes employing click chemistry. *J. Alloys Compd.* **2013**, *561*, 201–205. [CrossRef]
7. Tran, T.V.; Nguyen, D.T.C.; Le, H.T.N.; Tu, T.T.K.; Le, N.D.; Lim, K.T.; Bach, L.G.; Nguyen, T.D. MIL-53 (Fe)-directed synthesis of hierarchically mesoporous carbon and its utilization for ciprofloxacin antibiotic remediation. *J. Environ. Chem. Eng.* **2019**, *7*, 102881. [CrossRef]
8. Islam, M.R.; Bach, L.G.; Jung, S.J.; Lim, K.T. Facile Synthesis, Characterization, and Optical Properties of Ag+Doped ZnS Nanocrystals via Co-precipitation Method using Thioglycerol as a Capping Agent. *Mol. Cryst. Liq. Cryst.* **2013**, *583*, 134–140. [CrossRef]
9. Le, V.T.; Bach, L.G.; Pham, T.T.; Le, N.T.T.; Ngoc, U.T.P.; Tran, D.-H.N.; Nguyen, D.H. Synthesis and antifungal activity of chitosan-silver nanocomposite synergize fungicide against Phytophthora capsici. *J. Macromol. Sci. Part A* **2019**, *56*, 522–528. [CrossRef]
10. Haynes, C.L.; Van Duyne, R.P. Plasmon-Sampled Surface-Enhanced Raman Excitation Spectroscopy. *J. Phys. Chem. B* **2003**, *107*, 7426–7433. [CrossRef]
11. Zou, X.; Dong, S. Surface-Enhanced Raman Scattering Studies on Aggregated Silver Nanoplates in Aqueous Solution. *J. Phys. Chem. B* **2006**, *110*, 21545–21550. [CrossRef] [PubMed]
12. Lu, W.; Yao, K.; Wang, J.; Yuan, J. Ionic liquids–water interfacial preparation of triangular Ag nanoplates and their shape-dependent antibacterial activity. *J. Colloid Interface Sci.* **2015**, *437*, 35–41. [CrossRef] [PubMed]
13. Pal, S.; Tak, Y.K.; Song, J.M. Does the Antibacterial Activity of Silver Nanoparticles Depend on the Shape of the Nanoparticle? A Study of the Gram-Negative Bacterium Escherichia coli. *Appl. Environ. Microbiol.* **2007**, *73*, 1712–1720. [CrossRef] [PubMed]
14. Kelly, K.L.; Coronado, E.; Zhao, L.L.; Schatz, G.C. The Optical Properties of Metal Nanoparticles: The Influence of Size, Shape, and Dielectric Environment. *J. Phys. Chem. B* **2003**, *107*, 668–677. [CrossRef]
15. Sharma, V.K.; Yngard, R.A.; Lin, Y. Silver nanoparticles: Green synthesis and their antimicrobial activities. *Adv. Colloid Interface Sci.* **2009**, *145*, 83–96. [CrossRef]
16. Lok, C.-N.; Ho, C.-M.; Chen, R.; He, Q.-Y.; Yu, W.-Y.; Sun, H.; Tam, P.K.-H.; Chiu, J.-F.; Che, C.-M. Silver nanoparticles: partial oxidation and antibacterial activities. *J. Biol. Inorg. Chem.* **2007**, *12*, 527–534. [CrossRef]
17. Qing, Y.; Cheng, L.; Li, R.; Liu, G.; Zhang, B.; Tang, X.; Wang, J.; Liu, H.; Qin, Y. Potential antibacterial mechanism of silver nanoparticles and optimization of orthopedic implants by advanced modification technologies. *Int. J. Nanomed.* **2018**, *13*, 3311–3327. [CrossRef]
18. Seong, M.; Lee, D.G. Silver nanoparticles against Salmonella enterica serotype typhimurium: role of inner membrane dysfunction. *Curr. Microbiol.* **2017**, *74*, 661–670. [CrossRef]
19. Khalandi, B.; Asadi, N.; Milani, M.; Davaran, S.; Abadi, A.J.N.; Abasi, E.; Akbarzadeh, A. A review on potential role of silver nanoparticles and possible mechanisms of their actions on bacteria. *Drug Res. (Stuttg)* **2017**, *67*, 70–76. [CrossRef]
20. Zhao, R.; Lv, M.; Li, Y.; Sun, M.; Kong, W.; Wang, L.; Song, S.; Fan, C.; Jia, L.; Qiu, S.; et al. Stable nanocomposite based on PEGylated and silver nanoparticles loaded graphene oxide for long-term antibacte-rial activity. *ACS Appl. Mater. Interfaces* **2017**, *9*, 15328–15341. [CrossRef]
21. Gomaa, E.Z. Silver nanoparticles as an antimicrobial agent: a case study on Staphylococcus aureus and Escherichia coli as models for Gram-positive and Gram-negative bacteria. *J. Gen. Appl. Microbiol.* **2017**, *63*, 36–43. [CrossRef] [PubMed]
22. Siritongsuk, P.; Hongsing, N.; Thammawithan, S.; Daduang, S.; Klaynongsruang, S.; Tuanyok, A.; Patramanon, R. Two-phase bactericidal mechanism of silver nanoparticles against Burkholderia pseudomallei. *PLoS ONE* **2016**, *11*, e0168098.
23. Kvítek, L.; Panáček, A.; Soukupová, J.; Kolář, M.; Večeřová, R.; Prucek, R.; Holecová, M.; Zbořil, R. Effect of Surfactants and Polymers on Stability and Antibacterial Activity of Silver Nanoparticles (NPs). *J. Phys. Chem. C* **2008**, *112*, 5825–5834. [CrossRef]
24. Millstone, J.E.; Hurst, S.J.; Métraux, G.S.; Cutler, J.I.; Mirkin, C.A. Colloidal Gold and Silver Triangular Nanoprisms. *Small* **2009**, *5*, 646–664. [CrossRef]
25. Chen, S.; Carroll, D.L. Synthesis and Characterization of Truncated Triangular Silver Nanoplates. *Nano Lett.* **2002**, *2*, 1003–1007. [CrossRef]

26. Chen, S.; Fan, Z.; Carroll, D.L. Silver Nanodisks: Synthesis, Characterization, and Self-Assembly. *J. Phys. Chem. B* **2002**, *106*, 10777–10781. [CrossRef]
27. Sun, Y.; Mayers, B.; Xia, Y. Transformation of Silver Nanospheres into Nanobelts and Triangular Nanoplates through a Thermal Process. *Nano Lett.* **2003**, *3*, 675–679. [CrossRef]
28. Wang, C.-S.; Virgilio, N.; Wood-Adams, P.M.; Heuzey, M.-C. A gelation mechanism for gelatin/polysaccharide aqueous mixtures. *Food Hydrocoll.* **2018**, *79*, 462–472. [CrossRef]
29. de Kruif, C.G.; Weinbreck, F.; de Vries, R. Complex coacervation of proteins and anionic polysaccharides. *Curr. Opin. Colloid Interface Sci.* **2004**, *9*, 340–349. [CrossRef]
30. Suarasan, S.; Focsan, M.; Soritau, O.; Maniu, D.; Astilean, S. One-pot, green synthesis of gold nanoparticles by gelatin and investigation of their biological effects on Osteoblast cells. *Colloids Surfaces B Biointerfaces* **2015**, *132*, 122–131. [CrossRef]
31. Luo, Y.; Wang, Q. Recent development of chitosan-based polyelectrolyte complexes with natural polysaccharides for drug delivery. *Int. J. Biol. Macromol.* **2014**, *64*, 353–367. [CrossRef] [PubMed]
32. Lee, A.-C.; Hong, Y.-H. Coacervate formation of α-lactalbumin–chitosan and β-lactoglobulin–chitosan complexes. *Food Res. Int.* **2009**, *42*, 733–738. [CrossRef]
33. Li, Q.; Mahendra, S.; Lyon, D.Y.; Brunet, L.; Liga, M.V.; Li, D.; Alvarez, P.J.J. Antimicrobial nanomaterials for water disinfection and microbial control: Potential applications and implications. *Water Res.* **2008**, *42*, 4591–4602. [CrossRef] [PubMed]
34. Rabea, E.I.; Badawy, M.E.-T.; Stevens, C.V.; Smagghe, G.; Steurbaut, W. Chitosan as Antimicrobial Agent: Applications and Mode of Action. *Biomacromolecules* **2003**, *4*, 1457–1465. [CrossRef] [PubMed]
35. Ledwith, D.M.; Whelan, A.M.; Kelly, J.M. A rapid, straight-forward method for controlling the morphology of stable silver nanoparticles. *J. Mater. Chem.* **2007**, *17*, 2459–2464. [CrossRef]
36. Stevenson, K.; McVey, A.F.; Clark, I.B.N.; Swain, P.S.; Pilizota, T. General cabibration of microbial growth in microplate readers. *Sci. Rep.* **2016**, *6*. [CrossRef]
37. Bauer, A.W.; Kirby, W.M.M.; Sherris, J.C.; Turck, M. Antibiotic susceptibility testing by a standardized single disk method. *Am. J. Clin. Pathol.* **1966**, *36*, 493–496. [CrossRef]
38. Hudzicki, J. *Kirby-Bauer Disk Diffusion Susceptibility Test Protocol*; American Society for microbiology: Washington, DC, USA, 2009; pp. 1–23.
39. Lorian, V.; Atkinson, B.A. Determination of the range of antibacterial activity by use of viable counts. *J. Clin. Microbiol.* **1982**, *16*, 70–76.
40. Sanders, E.R. Aseptic Laboratory Techniques: Plating Methods. *J. Vis. Exp.* **2012**, *63*, 3064. [CrossRef]
41. Xue, C.; Mirkin, C.A. pH-Switchable Silver Nanoprism Growth Pathways. *Angew. Chem. Int. Ed.* **2007**, *46*, 2036–2038. [CrossRef]
42. Shuford, K.L.; Ratner, M.A.; Schatz, G.C. Multipolar excitation in triangular nanoprisms. *J. Chem. Phys.* **2005**, *123*, 114713. [CrossRef] [PubMed]
43. Lofton, C.; Sigmund, W. Mechanisms Controlling Crystal Habits of Gold and Silver Colloids. *Adv. Funct. Mater.* **2005**, *15*, 1197–1208. [CrossRef]
44. Wang, C.-S.; Natale, G.; Virgilio, N.; Heuzey, M.-C. Synergistic gelation of gelatin B with xanthan gum. *Food Hydrocoll.* **2016**, *60*, 374–383. [CrossRef]
45. Wang, X.-Y.; Wang, C.-S.; Heuzey, M.-C. Complexation of chitosan and gelatin: From soluble complexes to colloidal gel. *Int. J. Polym. Mater. Polym. Biomater.* **2016**, *65*, 96–104. [CrossRef]
46. Pelc, D.; Marion, S.; Požek, M.; Basletić, M. Role of microscopic phase separation in gelation of aqueous gelatin solutions. *Soft Matter* **2014**, *10*, 348–356. [CrossRef]
47. Zhang, W.; Huang, Y.; Wang, W.; Huang, C.; Wang, Y.; Yu, Z.; Zhang, H. Influence of pH of Gelatin Solution on Cycle Performance of the Sulfur Cathode. *J. Electrochem. Soc.* **2010**, *157*, A443–A446. [CrossRef]
48. Torii, H. *Theoretical Analyses of the Amide I Infrared Bands of Globular Proteins, Infrared Spectroscopy of Biomolecules*; Tasumi, M., Mantsch, H.H., Chapman, D., Eds.; Wiley-Liss Inc.: Flatbush, NY, USA, 1996; Chapter 1.
49. Venkatesham, M.; Ayodhya, D.; Madhusudhan, A.; Babu, .N.V.; Veerabhadram, G. A novel green one-step synthesis of silver nanoparticles using chitosan; catalytic activity and antimicrobial studies. *Appl. Nanosci.* **2012**, *4*, 113–119. [CrossRef]
50. Antoniades, M.G.; Wey, J.S. The effect of coalescence on AgBr tabular grain formation. *J. Imaging Sci. Technol.* **1995**, *39*, 323–331.

51. Morones, J.R.; Elechiguerra, J.L.; Camacho, A.; Holt, K.; Kouri, J.B.; Ramírez, J.T.; Yacaman, M.J. The bactericidal effect of silver nanoparticles. *Nanotechnology* **2005**, *16*, 2346–2353. [CrossRef]
52. Hwang, E.; Lee, J.; Chae, Y.; Kim, Y.; Kim, B.; Sang, B.; Gu, M. Analysis of the toxic mode of action of silver nanoparticles using stress-specific bioluminescent bacteria. *Small* **2008**, *4*, 746–750. [CrossRef]